

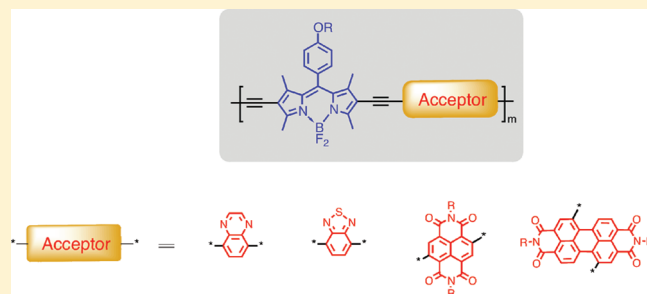
BODIPY-Based Donor–Acceptor π -Conjugated Alternating Copolymers

Bhooshan C. Popere, Andrea M. Della Pelle, and S. Thayumanavan*

Department of Chemistry, University of Massachusetts, Amherst, Massachusetts 01003, United States

Supporting Information

ABSTRACT: Four novel π -conjugated copolymers incorporating 4,4-difluoro-4-borata-3a-azonia-4a-aza-s-indacene (BODIPY) core as the “donor” and quinoxaline (Qx), 2,1,3-benzothiadiazole (BzT), *N,N'*-di(2'-ethyl)hexyl-3,4,7,8-naphthalenetetracarboxylic diimide (NDI), and *N,N'*-di(2'-ethyl)hexyl-3,4,9,10-perylene tetracarboxylic diimide (PDI) as acceptors were designed and synthesized via Sonogashira polymerization. The polymers were characterized by ^1H NMR spectroscopy, gel permeation chromatography (GPC), UV–vis absorption spectroscopy, and cyclic voltammetry. Density functional theory (DFT) calculations were performed on polymer repeat units, and the highest occupied molecular orbital (HOMO) and the lowest unoccupied molecular orbital (LUMO) energy levels were estimated from the optimized geometry using B3LYP functional and 6-311g(d,p) basis set. Copolymers with Qx and BzT possessed HOMO and LUMO energy levels comparable to those of BODIPY homopolymer, while PDI stabilized both HOMO and LUMO levels. Semiconductor behavior of these polymers was estimated in organic thin-film transistors (OTFT). While the homopolymer, Qx, and BzT-based copolymers showed only p-type semiconductor behavior, copolymers with PDI and NDI showed only n-type behavior.



INTRODUCTION

4,4-Difluoro-4-borata-3a-azonia-4a-aza-s-indacene dyes, more commonly known as BODIPY dyes, have been long since recognized for their excellent optical properties such as large absorption coefficients, high fluorescence quantum yields, and remarkable photostability.¹ Additionally, straightforward chemical synthesis and structural robustness have enabled fine-tuning of optical properties of BODIPY dyes via systematic structural variations. For instance, small-molecule BODIPY derivatives with solution-state absorption maxima ranging from 500 to 700 nm have been reported and are commonly used in biological imaging.² Additionally, the optical properties, ease of synthetic modification, and chemical and photostability make BODIPY-based systems attractive candidates for light-harvesting applications.³ Owing to large extinction coefficients, intense absorption spectra that extend into the red region of the visible spectrum, and decent hole mobility, small-molecule BODIPY derivatives have been recently employed as p-type or donor materials in conjunction with PCBM in bulk heterojunction (BHJ) solar cells.⁴

π -Conjugated polymers based on the BODIPY core naturally extend the absorption into the deep-red regions of the visible spectrum and, in some cases, are excellent near-infrared emitters.⁵ The relatively high extinction coefficients of these polymers combined with their photostability make them attractive candidates for optoelectronic applications, specifically polymeric photovoltaics.⁶ On the basis of the prior knowledge that small molecule BODIPY derivatives function as electron donors in BHJ

solar cells, it is reasonable to assume that the corresponding homopolymers involving the BODIPY core in the π -conjugated backbone should also function as donor polymers in polymer–PCBM BHJ solar cells. Indeed, an ethynyl-bridged alternating copolymer of BODIPY with thiophene has shown electron donor characteristics in BHJ solar cells. The optical bandgap of the resulting copolymer, however, was identical to that of the homopolymer.⁷

The electrochemical characteristics of several small-molecule BODIPY derivatives show excellent reversibility during both oxidation and reduction.⁸ To us, this implies that the BODIPY core is capable of stabilizing an additional electron as well as a hole, both in small molecules and in π -conjugated polymers. Indeed, the cyclic voltammogram of our BODIPY-based homopolymer (*vide infra*) clearly indicates both reduction and oxidation behavior in thin films. This provides us with a unique and rare opportunity to systematically study the effect of different electron-rich or electron-poor comonomers on the optical and electrochemical properties of BODIPY-based conjugated alternating copolymers, which is currently lacking in the literature.

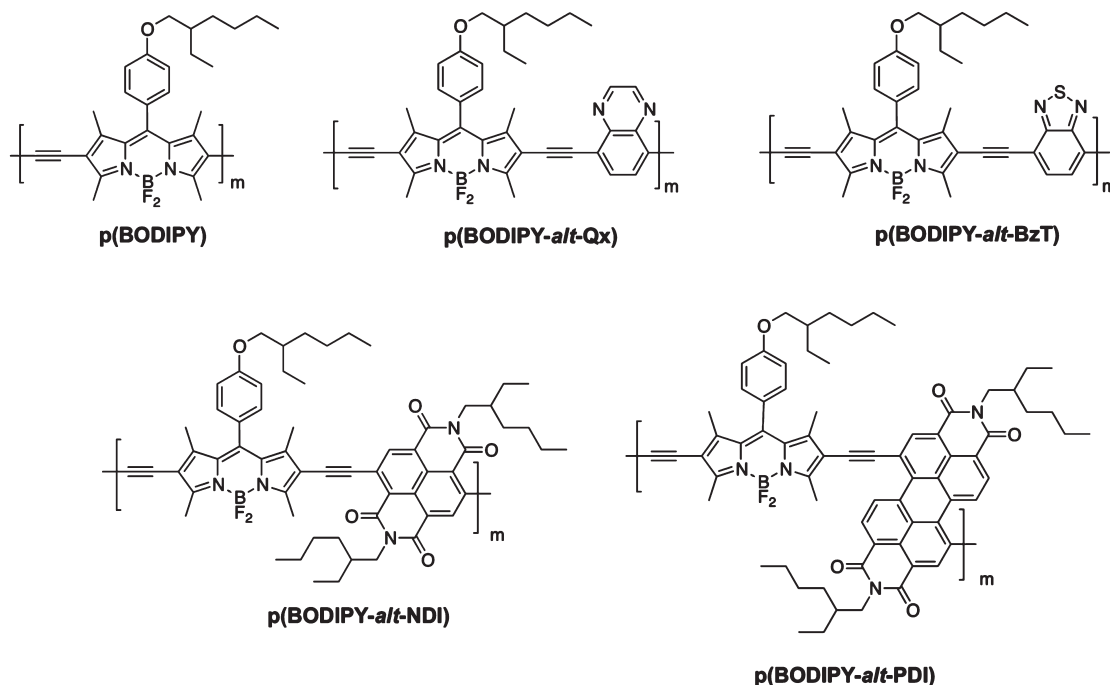
Several acceptor units have been designed synthesized and used in conjunction with various donor segments, effecting reduced bandgaps in the resulting π -conjugated polymers.⁹ Although the end result of most D–A combinations has been

Received: April 11, 2011

Revised: May 6, 2011

Published: May 19, 2011

Chart 1. Chemical Structures of the Synthesized BODIPY-Based Homopolymer and Copolymers



a reduced bandgap compared to the corresponding donor homopolymers, each combination has a unique set of properties.¹⁰ Among the myriad of acceptor units studied so far, *o*-quinoid acceptors¹¹ such as 2,1,3-benzothiadiazole,¹² quinoxaline,^{12g,13} thieno[3,4-*b*]pyrazine,^{10g,14} benzo[1,2-*c*,4,5-*c'*]bis[1,2,5]thiadiazole,¹⁵ and [1,2,5]thiadiazolo[3,4-*g*]quinoxaline^{11b,16} have garnered much attention. Alternating copolymers made from aromatic donors and these *o*-quinoid acceptor heterocycles are highly polarized and possess small HOMO–LUMO gaps, leading to absorption spectra extending into the near-infrared region.

Second, small-molecule and polymeric systems based on *N,N'*-dialkyl-1,4,5,8-naphthalenetetracarboxylic diimide (NDI)¹⁷ and *N,N'*-dialkyl-3,4,9,10-perylenetetracarboxylic diimide (PDI)¹⁸ have been demonstrated to possess excellent electron mobility.¹⁹ However, reports on alternating D–A type copolymers synthesized using these rylene acceptors are rather scarce compared with *o*-quinoid acceptors. In addition to possessing reduced optical bandgaps, the copolymers based on π -conjugated PDI or NDI units (substituted through the aromatic core) show excellent electron transport characteristics.²⁰ Consequently, these polymers have been used as fullerene substitutes in all-polymer organic solar cells with reduced optical bandgaps, broadened absorption across the visible spectrum, and deep HOMO and LUMO energy levels.²¹

In light of the above discussion, we have designed, synthesized, and characterized four BODIPY–acceptor alternating π -conjugated polymers (Chart 1). We have chosen two acceptor units each from the *o*-quinoid and rylene type acceptors. Quinoxaline (Qx) and 2,1,3-benzothiadiazole (BzT) constitute the *o*-quinoid acceptors, while *N,N'*-di(2-ethyl)hexyl-1,4,5,8-naphthalenetetracarboxylic diimide and *N,N'*-di(2-ethyl)hexyl-3,4,9,10-perylenetetracarboxylic diimide (PDI) constitute the rylene acceptors. Steady-state UV–vis absorption spectroscopy and thin film cyclic voltammetry were used to determine the optical and electrochemical characteristics of these polymers. To gain a

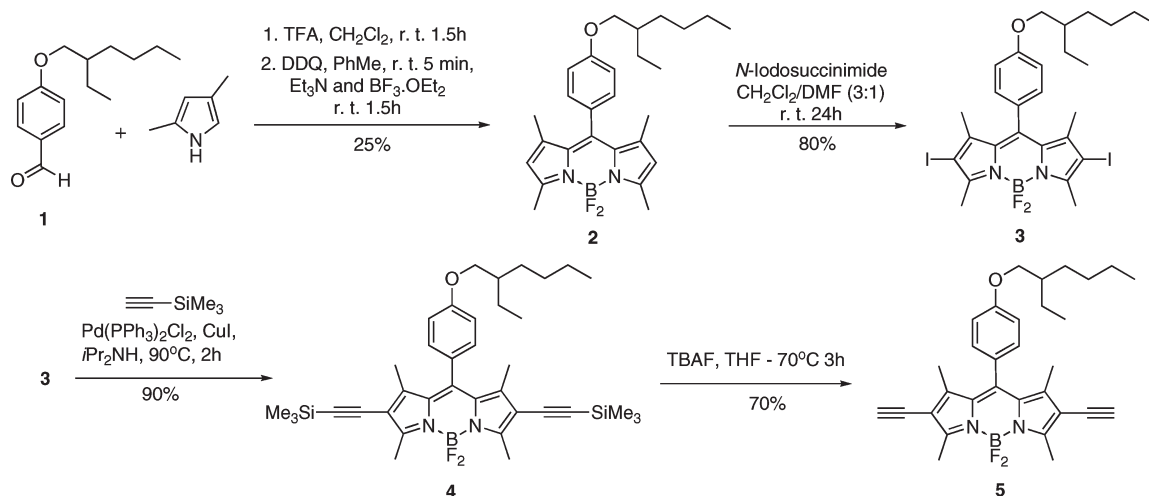
deeper insight into the peculiar characteristics of each of these polymers, we have performed DFT calculations on the respective model compounds that constitute the repeating units of the corresponding polymers. Furthermore, semiconductor behavior of these polymers was evaluated using thin-film field-effect transistor measurements.

RESULTS AND DISCUSSION

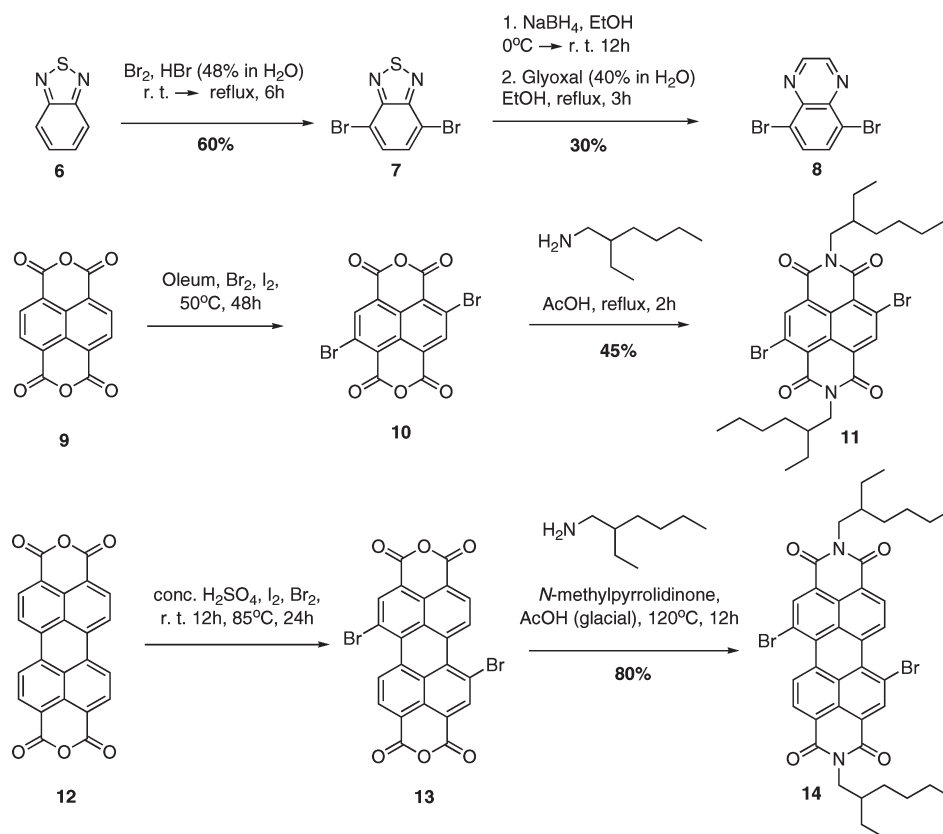
Synthesis and Characterization. To synthesize the targeted polymers, we first synthesized the corresponding monomer units. 2,6-Diethynyl BODIPY was synthesized according to the reported procedure with small modifications wherever necessary as outlined in Scheme 1.⁶ Briefly, condensation of 4-(2'-ethyl)hexyloxybenzaldehyde (**1**) with 2,4-dimethylpyrrole gave the corresponding dipyrromethane. This was then oxidized by DDQ to generate dipyrromethene followed by coordination with trifluoroborane dietherate to give the BODIPY core (**2**) in 25% overall yield. Iodination of the BODIPY core at the 2- and 6-position using *N*-iodosuccinimide yielded 2,6-diiodo BODIPY (**3**) in about 80% yield. This was then subjected to Pd(II)- and CuI-catalyzed Sonogashira cross-coupling reaction with trimethylsilyl (TMS) acetylene to generate 2,6-bis(trimethylsilylethynyl) BODIPY (**4**). The TMS groups were subsequently deprotected using tetrabutylammonium fluoride at reduced temperatures to finally yield 2,6-diethynyl BODIPY (**5**). It is important to carry out this reaction at reduced temperatures because the diacetylide anions generated during this reaction are nucleophilic enough to react with the boron center at room temperature and thereby replace the fluorine atoms irreversibly.²²

Scheme 2 outlines the synthesis of the *o*-quinoid acceptor units, namely 4,7-dibromo-2,1,3-benzothiadiazole and dibromoquinoxaline. 2,1,3-Benzothiadiazole (**6**) was subjected to bromination under acidic conditions according to a previously reported

Scheme 1. Synthesis of BODIPY Monomer



Scheme 2. Syntheses of Acceptor Monomers

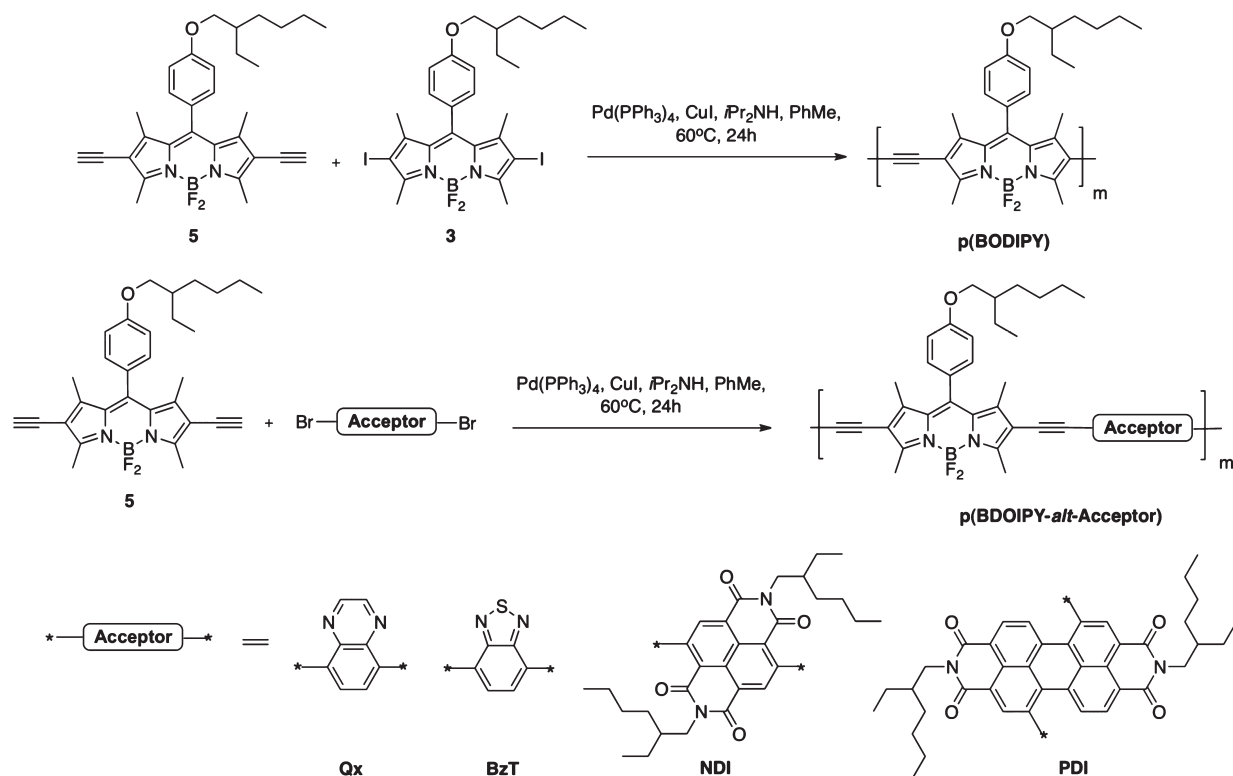


procedure to yield the corresponding dibromo compound **7**.¹³ Desulfurization of 4,7-dibromo-2,1,3-benzothiadiazole resulted in the 2-amino-3,6-dibromoaniline intermediate that was then condensed *in situ* with glyoxal to give dibromoquinoxaline (**8**) in moderate yields.²³

N,N'-Di(2-ethyl)hexyl-2,6-dibromo-1,4,5,8-naphthalene-tetracarboxylic diimide (**11**) diimide was synthesized by first brominating the corresponding anhydride (**9**) using fuming

sulfuric acid and bromine.²⁴ Reaction of the corresponding dibromo dianhydride (**10**) with 2-ethylhexylamine gave compound **11** in moderate yields. Similarly, *N,N'*-di(2'-ethyl)hexyl-1,7-dibromo-3,4,9,10-perylenetetracarboxylic diimide (**14**) was synthesized according to a previously reported protocol.²⁵ Briefly, 3,4,9,10-perylenetetracarboxylic acid dianhydride (**12**) was brominated under hot sulfuric acid conditions in the presence of a catalytic amount of molecular iodine. This reaction

Scheme 3. Syntheses of BODIPY-Based Polymers via Sonogashira Polymerization



yielded a product mixture primarily comprising of the desired 1,7-dibromo isomer, along with, 1,6-dibromo and the 1,6,7-tribromo PTCDA isomers that could not be separated at this stage. Imidation with 2-ethylhexylamine in hot *N*-methylpyrrolidinone yielded the corresponding imides. Once again, the product of this reaction contained a mixture of the 1,7-dibromo and the 1,6-dibromo PDI isomers that were used as such. The ratio of 1,7- and 1,6- isomers was found to be 80:20 as investigated by ^1H NMR spectroscopy (See Supporting Information).

All the polymers were synthesized via the Sonogashira condensation polymerization reaction using 1:1 monomer feed ratios. In a typical experiment, 2,6-diethynyl BODIPY was reacted with the corresponding dihalide in presence of $\text{Pd(PPh}_3)_4$ and CuI to yield the corresponding polymer. The polymerizations were carried out in a degassed mixture of anhydrous diisopropylamine and anhydrous toluene at 60°C for 24 h. The crude polymers were precipitated from methanol, filtered, and dried. In each case, the crude polymer was then purified by Soxhlet extraction with methanol, acetone, and chloroform. The chloroform fraction was then concentrated under reduced pressure, reprecipitated from methanol, filtered, and dried to yield a deep violet to deep blue polymer. The resulting polymers were readily soluble in chloroform, THF, chlorobenzene, and *o*-dichlorobenzene.

The polymers were characterized with ^1H NMR spectroscopy and gel permeation chromatography (GPC). The proton signals in the NMR spectra were broadened compared to the monomers indicative of successful polymerization of the monomers. For copolymers, integration of the proton signals in the aromatic region indicated 1:1 polymer composition. The molecular weights of the polymers were estimated by GPC using THF as the mobile phase and calibrated against polystyrene standards (Table 1).

Table 1. Molecular Weights of the BODIPY-Based Conjugated Polymers

polymer	M_n^a [g/mol]	M_w^a [g/mol]	PD ^a
p(BODIPY)	4200	7100	1.69
p(BODIPY-alt-Qx)	2900	4300	1.48
p(BODIPY-alt-BzT)	2300	3200	1.39
p(BODIPY-alt-NDI)	4000	8200	2.05
p(BODIPY-alt-PDI)	4100	9200	2.24

^a M_n , M_w , and PD of polymers were determined by GPC using polystyrene standards with THF as eluent.

Optical Properties. The UV–vis absorption spectra of the polymers in dilute chloroform solutions and as thin films are shown in Figure 1. Steady-state absorption spectra of p(BODIPY), p(BODIPY-alt-Qx), and p(BODIPY-alt-BzT) show two distinct absorption bands: a high-energy band between 350 and 475 nm that is relatively independent of the nature of the acceptor units and a low-energy band between 500 and 750 nm that is characteristic of all BODIPY-based conjugated polymers.⁶ The high intensity of this band reflects the large extinction coefficient of the BODIPY core. The absorption maxima of p(BODIPY), p(BODIPY-alt-Qx), and p(BODIPY-alt-BzT) in chloroform solutions at room temperature are 656, 596, and 604 nm, respectively, while the corresponding absorption onsets are at 690, 640, and 650 nm, respectively. It is interesting to note that the absorption spectra of p(BODIPY-alt-Qx) and p(BODIPY-alt-BzT) show a considerable blue shift relative to that of p(BODIPY). This is contrary to other π -conjugated polymers that incorporate BzT and Qx as “acceptor” units.^{13d,e,g}

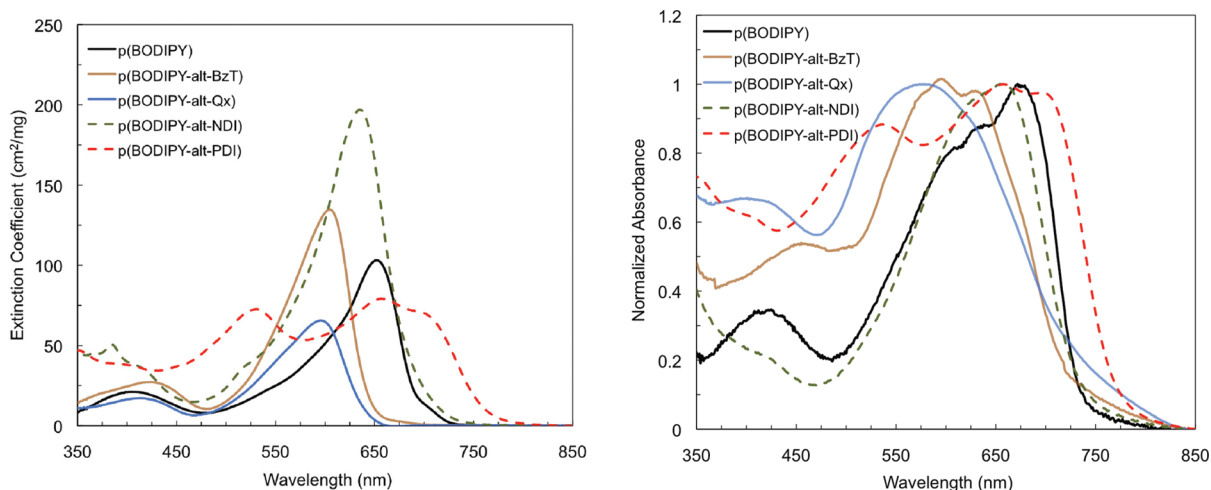


Figure 1. UV-vis absorption spectra of BODIPY-based polymers represented as extinction coefficients in chloroform solutions (left) and normalized absorption in thin films annealed at 100 °C (right).

Table 2. Summary of Optical Properties of BODIPY-Based Conjugated Polymers

polymer	solution		thin films				$E_g^{\text{opt}^a}$ [eV]	$E_g^{\text{elec}^b}$ [eV]
	λ_{max} [nm]	λ_{onset} [nm]	as cast		annealed			
			λ_{max} [nm]	λ_{onset} [nm]	λ_{max} [nm]	λ_{onset} [nm]		
p(BODIPY)	656	690	670	735	678	745	1.66	1.86
p(BODIPY- <i>alt</i> -Qx)	596	640	595	712	593	750	1.65	1.75
p(BODIPY- <i>alt</i> -BzT)	604	650	634	720	598	740	1.67	1.86
p(BODIPY- <i>alt</i> -NDI)	634	715	618	732	660	762	1.63	1.79
p(BODIPY- <i>alt</i> -PDI)	656	765	656	770	660	788	1.57	1.67

^a E_g^{opt} calculated from the intersection of the tangent drawn to the lowest energy absorption edge with the baseline in annealed thin films. ^b E_g^{elec} = LUMO^{elec} – HOMO^{elec} as determined from cyclic voltammetry (*vide infra*).

However, the corresponding absorption spectra in annealed thin films are significantly broadened and red-shifted (~ 50 nm) compared to the solution-state spectra, presumably due to planarization of the polymer backbone and enhanced interchain interactions in solid state. Thin-film spectra of p(BODIPY) and p(BODIPY-*alt*-BzT) show additional features, while that of p(BODIPY-*alt*-Qx) remains featureless. Conservatively estimated optical bandgaps from the low-energy absorption edges for p(BODIPY), p(BODIPY-*alt*-Qx), and p(BODIPY-*alt*-BzT) are 1.66, 1.65, and 1.67 eV, respectively.

The solution-state absorption spectrum of p(BODIPY-*alt*-NDI) shows a global maximum at 634 nm while the corresponding absorption onset is at 715 nm. In thin films, the absorption maximum and the onset red shift to 660 and 762 nm, respectively, implying planarization of the polymer backbone in the solid state. The absorption spectrum of p(BODIPY-*alt*-PDI), however, is markedly different from all the other polymers discussed above in several ways. First, in addition to the BODIPY-based transition at 656 nm, we see a distinct low-energy band centered at 715 nm in solution that can be attributed to the BODIPY-to-PDI intramolecular charge-transfer (ICT) transition that tails off into the deep-red region of the spectrum. Furthermore, contrary to most low bandgap conjugated polymers, the intensity of this ICT band is comparable to the most

intense feature in the absorption spectrum. Second, we also see a distinct band between 450 and 575 nm that can be attributed to the PDI-based transition.^{21b,26} Once again, owing to the large extinction coefficient of the PDI core, the intensity of this feature is comparable to that of the BODIPY-based transition. Thus, p(BODIPY-*alt*-PDI) shows a uniform absorption spectrum that spans over most of the visible spectrum. Third, we do not see any bathochromic shift in the solid-state absorption spectrum. This could be due to the lack of further planarization of the polymer backbone. This has been observed with a few examples of conjugated polymers employing PDI units in their backbone.²⁶ The optical bandgap of p(BODIPY-*alt*-PDI) estimated from the absorption onset in the red region is 1.57 eV.

Electrochemical Properties. The redox properties of BODIPY-based polymers were evaluated using cyclic voltammetry. Polymer films were drop-cast from chloroform solutions onto a 2 mm diameter Pt disk electrode. The cyclic voltammograms were recorded against Ag/Ag⁺ reference electrode in anhydrous acetonitrile with 0.1 M tetrabutylammonium hexafluorophosphate (TBAPF₆) as the supporting electrolyte at a scan rate of 50 mV/s. The electrochemical potentials were estimated from the onset of the oxidation and reduction sweeps. All voltammograms were calibrated using the Fc/Fc⁺ redox couple. The redox potentials thus obtained were converted to the corresponding

energy levels assuming the absolute HOMO energy level of ferrocene to be -4.8 eV²⁷ (eq 1).

$$\begin{aligned} \text{HOMO} &= -(E_{\text{ox}, \text{onset}} + 4.8) \text{ eV} \\ \text{LUMO} &= -(E_{\text{red}, \text{onset}} + 4.8) \text{ eV} \end{aligned} \quad (1)$$

The onset oxidation and reduction potentials along with the estimated HOMO and LUMO energy levels are summarized in Table 3 for comparison, while the representative scans of the polymer thin films are shown in Figure 2. The voltammograms are displaced along the y -axis for clarity. All polymers show irreversible oxidation and quasi-reversible reduction behavior. Evidently, the redox potentials for p(BODIPY-*alt*-Qx) and p(BODIPY-*alt*-BzT) copolymers bear strong resemblance to the that of p(BODIPY). Furthermore, the reduction scans of all three polymers show a distinct peak at ~ -1.5 V that is characteristic of the BODIPY reduction. The HOMO energy levels of p(BODIPY), p(BODIPY-*alt*-Qx), and p(BODIPY-*alt*-BzT) are -5.33 , -5.33 , and -5.44 eV, respectively, while the corresponding LUMO energy levels are -3.47 , -3.58 , and -3.58 eV, respectively. The electrochemical data and the optical data unambiguously indicate that BzT and Qx as acceptor units do not significantly perturb the HOMO and LUMO energy levels of the corresponding copolymers compared with the energy levels of p(BODIPY) (Figure 2).

p(BODIPY-*alt*-NDI) and p(BODIPY-*alt*-PDI), on the other hand, show markedly different redox chemistry compared with the other polymers in the series. Both polymers show

Table 3. Summary of Electrochemical Data for BODIPY-Based Polymers

polymer	$E^{\text{ox}a}$ [V]	HOMO ^{elec b} [eV]	$E^{\text{red}a}$ [V]	LUMO ^{elec b} [eV]
p(BODIPY)	+0.64	-5.33	-1.22	-3.47
p(BODIPY- <i>alt</i> -Qx)	+0.64	-5.33	-1.11	-3.58
p(BODIPY- <i>alt</i> -BzT)	+0.75	-5.44	-1.11	-3.58
p(BODIPY- <i>alt</i> -NDI)	+0.86	-5.55	-0.93	-3.76
p(BODIPY- <i>alt</i> -PDI)	+1.04	-5.73	-0.60	-4.09

^a E^{ox} and E^{red} determined from the onset potentials of the oxidation and reduction waves, respectively. ^b HOMO^{elec} = $-(E^{\text{ox}} + 4.8)$ eV and LUMO^{elec} = $-(E^{\text{red}} + 4.8)$ eV.

characteristic features of the respective rylene diimide in the reduction scans of the cyclic voltammograms. p(BODIPY-*alt*-NDI) shows two characteristic quasi-reversible reductions, the first of which corresponds to reduction of NDI²⁸ and the peak around -1.5 V corresponds to the reduction of the BODIPY core. Similarly, p(BODIPY-*alt*-PDI) shows three quasi-reversible reduction peaks, the first two of which can be assigned to PDI-centered reduction while the last one is characteristic of BODIPY-based reduction as discussed above.²⁹ Both NDI and PDI small molecules typically show two distinct reversible reduction peaks. However, in the case of p(BODIPY-*alt*-NDI), we were unable to see these two reduction peaks. It is possible that the second reduction of NDI core and the reduction of the BODIPY core occur around the same potential. We did not see any additional peaks even at a lower scan rate (10 mV/s). The HOMO energy levels thus estimated for p(BODIPY-*alt*-NDI) and p(BODIPY-*alt*-PDI) are -5.55 and -5.73 eV, respectively, while the corresponding LUMO energy levels are -3.76 and -4.09 eV. It is gratifying to note that introduction of the PDI units in the polymer backbone causes significant stabilization of the HOMO and LUMO energy levels with a concurrent reduction in the optical and electrochemical bandgaps.²⁶ Although introducing NDI unit in the polymer backbone does not effectively reduce the HOMO–LUMO separation of p(BODIPY-*alt*-NDI), the resulting molecular orbitals are relatively stabilized compared with p(BODIPY), p(BODIPY-*alt*-Qx), and p(BODIPY-*alt*-BzT).

Theoretical Calculations. In order to gain a deeper insight into the optical and electrochemical properties of our polymers, we performed density functional theory (DFT) analysis on model compounds constituting the corresponding repeat units. HOMO and LUMO energy levels were estimated from the optimized geometry using B3LYP functional and 6-311g(d,p) basis set. The surface plots for the model compounds are shown in Figure 3 for comparison. In principle, the HOMO and LUMO energy levels of D–A type conjugated polymers depend on the relative placement of the HOMO and LUMO energy levels of the respective donor and acceptor segments. Our calculations suggest that the LUMO energy levels of Qx (-2.62 eV) and BzT (-2.97 eV) lie very close to and, in the case of Qx, slightly above the LUMO energy level of BODIPY (-2.90 eV). This implies that BODIPY has a comparable electron affinity with Qx and

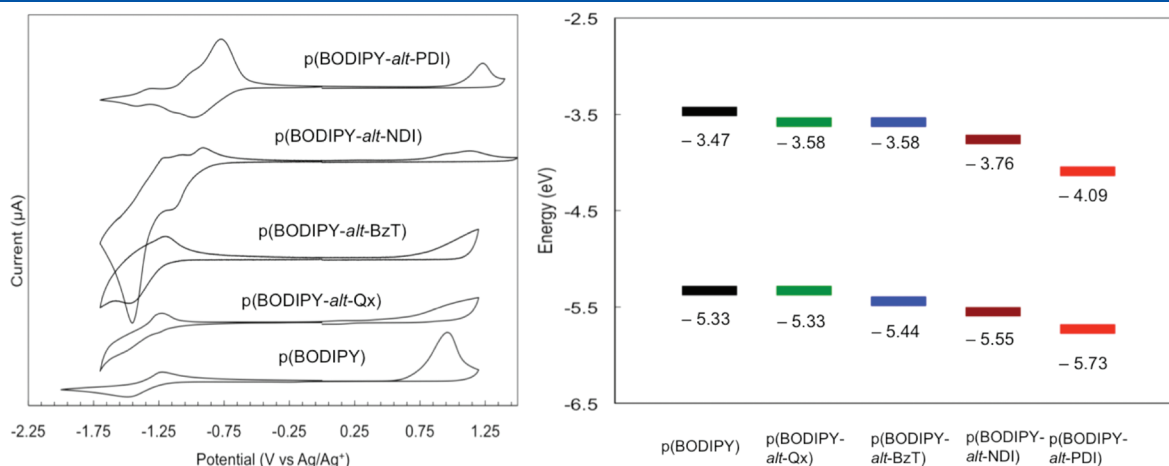


Figure 2. Cyclic voltammograms of all the polymers cast as thin films from chloroform solutions on platinum disk electrode (left) and comparative HOMO and LUMO energy levels thus estimated (right).

BzT, which reflects in the almost identical optical bandgaps for all the three polymers: p(BODIPY), p(BODIPY-*alt*-Qx), and p(BODIPY-*alt*-BzT). Our DFT calculations indicate that in the case of BODIPY-Qx and BODIPY-BzT models both HOMO and LUMO wave functions are delocalized with significant contribution to the LUMO from the BODIPY core (Figure 3). This is also reflected in the cyclic voltammograms of the polymers that predominantly show redox potentials corresponding to the BODIPY core (Figure 3).

On the other hand, the calculated LUMO energy level of PDI is -3.68 eV, and hence, it has a higher electron affinity compared to BODIPY. Thus, in principle, PDI can act as an acceptor while used in conjunction with BODIPY while designing conjugated polymers with reduced optical bandgaps. This is evident from the absorption and electrochemical features discussed above. The HOMO wave function in the case of BODIPY-PDI model is extensively delocalized along the backbone, while the LUMO resides on the PDI unit. This feature is characteristic of most donor-acceptor polymers reported in the literature.³⁰

Although the calculated LUMO energy level of NDI (-3.69 eV) is lower than that of BODIPY and almost comparable to that of PDI, the absorption spectrum of p(BODIPY-*alt*-NDI) does not show an ICT band as observed in p(BODIPY-*alt*-PDI). Our calculations on BODIPY-NDI units show that there is significant orbital partitioning between the two components. While the HOMO is primarily BODIPY-centered, the LUMO wave

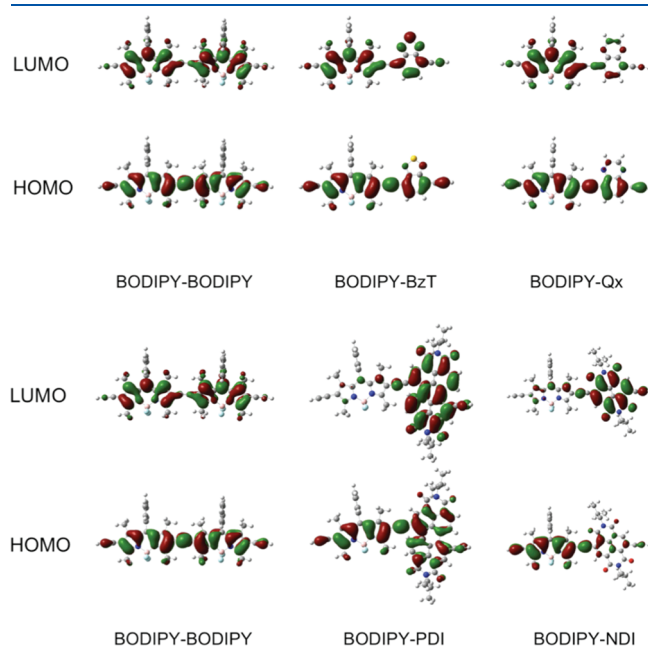


Figure 3. HOMO and LUMO surface plots for BODIPY-acceptor model compounds.

Table 4. Summary of Field-Effect Mobilities for BODIPY-Based Conjugated Polymers Determined from Bottom-Contact Thin-Film Transistors

polymer	μ_{\max} [$\text{cm}^2/(\text{V s})$]	μ_{avg} [$\text{cm}^2/(\text{V s})$]	V_t [V]	$I_{\text{on/off}}$
p(BODIPY)	2.9×10^{-6} (h^+)	2.3×10^{-6} ($\pm 4.8 \times 10^{-7}$, h^+)	-75	10^3
p(BODIPY- <i>alt</i> -Qx)	1.6×10^{-9} (h^+)	1.7×10^{-10} ($\pm 5.5 \times 10^{-10}$, h^+)	-53	10^2
p(BODIPY- <i>alt</i> -BzT)	3.1×10^{-8} (h^+)	2.2×10^{-8} ($\pm 9.3 \times 10^{-9}$, h^+)	-44	10^2
p(BODIPY- <i>alt</i> -NDI)	3.9×10^{-6} (e^-)	3.7×10^{-6} ($\pm 2.3 \times 10^{-7}$, e^-)	$+43$	10^3
p(BODIPY- <i>alt</i> -PDI)	1.4×10^{-5} (e^-)	1.3×10^{-5} ($\pm 6.4 \times 10^{-7}$, e^-)	$+37$	10^4

function resides almost entirely on the NDI core, resulting in an ineffective orbital mixing. Thus, there seems to be very poor intramolecular π -electron delocalization along the polymer backbone in p(BODIPY-*alt*-NDI). This explains why although having comparable electron affinity, PDI and NDI have different effect on the energy levels of the resulting copolymers.

Thus, as seen from optical and electrochemical measurements and theoretical calculations, both PDI and NDI cause a net stabilization of HOMO and LUMO energy levels. This is not unusual for rylene-based acceptors, as they are known to exert strong electron-withdrawing forces thereby lowering the LUMO energy levels, making the resulting copolymers efficient n-type semiconductors. We believe that the broad absorption spectrum, large extinction coefficients in the entire visible region, and reduced bandgap could make p(BODIPY-*alt*-PDI) and p(BODIPY-*alt*-NDI) potentially useful as electron transporting materials.

Charge Carrier Mobility Measurements. We investigated the ability of our BODIPY-based polymers to behave as both p-type and n-type semiconductors by analyzing the charge carrier mobility in thin films using the field-effect transistor configuration. Bottom-contact field-effect transistors were fabricated by spin-coating 10 mg/mL polymer solutions from chlorobenzene onto octadecyltrimethoxysilane (OTS) treated, heavily doped SiO_2/Si substrates. The substrates were annealed at 80°C for 1 h before analyzing them for charge carrier mobility. All the measurements were performed in a glovebox under an argon atmosphere, and the results are summarized in Table 4. The charge carrier mobilities were calculated from the saturation regime using the following equation:

$$I_D = (\mu C_i W/2L)[(V_{GS} - V_t)]$$

Analogous with small-molecule and polymeric BODIPY derivatives, p(BODIPY), p(BODIPY-*alt*-BzT), and p(BODIPY-*alt*-Qx) showed p-type semiconductor behavior. The hole mobility for p(BODIPY) was found to be $\sim 3 \times 10^{-6} \text{ cm}^2/(\text{V s})$, which is comparable to the previously reported value.⁷ The incorporation of BzT and Qx in the polymer backbone decreased the hole mobility by a few orders of magnitude. On the other hand, p(BODIPY-*alt*-NDI) and p(BODIPY-*alt*-PDI) showed n-type semiconductor behavior. The saturation regime electron mobility for p(BODIPY-*alt*-NDI) was found to be $\sim 4 \times 10^{-6} \text{ cm}^2/(\text{V s})$, while that for p(BODIPY-*alt*-PDI) was an order of magnitude higher ($\sim 1.5 \times 10^{-5} \text{ cm}^2/(\text{V s})$) (Figure 4). Although the mobilities are relatively modest compared with some other PDI-based n-type semiconducting polymers,^{20a,c} to the best of our knowledge, p(BODIPY-*alt*-NDI) and p(BODIPY-*alt*-PDI) are the only polymers based on the BODIPY core that show any n-channel activity. This supports our hypothesis that p(BODIPY-*alt*-PDI) and p(BODIPY-*alt*-NDI) could potentially

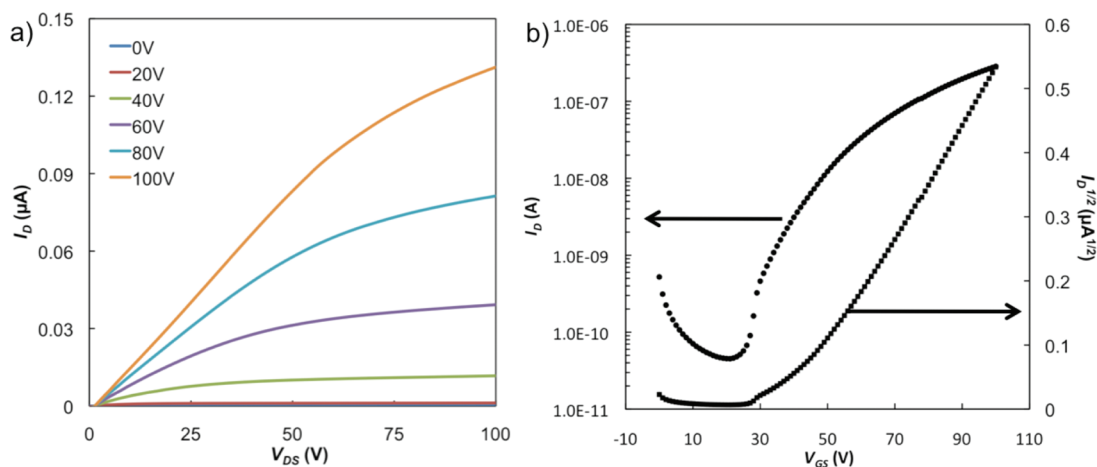


Figure 4. Output characteristics (left) and transfer characteristics (right) for p(BODIPY-*alt*-PDI)-based bottom-gate bottom-contact thin-film field-effect transistors at $W/L = 2000$.

be useful as n-type semiconducting materials. The output characteristics show saturation behavior at a channel length of $5 \mu\text{m}$, an on/off ratio of about 10^3 , and a threshold voltage of about 35 V.

CONCLUSIONS

In summary, we have successfully synthesized and characterized four alternating π -conjugated polymers based on the BODIPY core utilizing *o*-quinoid acceptors like quinoxaline and benzothiadiazole, and rylene acceptors like NDI and PDI. The optical and electrochemical properties of the BODIPY-acceptor conjugated polymers depend on the electron affinity of the corresponding acceptor units. While units with comparable electron affinity to BODIPY do not significantly perturb the energy levels of the corresponding copolymers, stronger acceptor units like PDI tend to bring out the relative electron donor characteristics of the BODIPY core. These polymers can be considered low bandgap polymers with low-lying HOMO energy level. UV-vis absorption spectra of these polymers reflect the characteristics of the BODIPY core. Specifically, the absorption spectrum of p(BODIPY-*alt*-PDI) spans most of the visible spectrum (350–800 nm) while retaining the intense absorption characteristics of both BODIPY and PDI units. Preliminary charge transport measurements indicate that BODIPY-based conjugated polymers can be active as both p-type and n-type semiconductors and that the switch between p-type and n-type can be accomplished by a choice of suitable comonomers. Thus, we believe that p(BODIPY-*alt*-PDI) holds a strong potential to function as an efficient n-type semiconducting polymer, with stable energy levels, reduced optical bandgap, and panchromatic absorption.

EXPERIMENTAL SECTION

Instrumentation. ^1H NMR spectra were recorded on a 400 MHz Bruker NMR spectrometer using the residual proton resonance of the solvent as the internal standard. Chemical shifts are reported in parts per million (ppm). When peak multiplicities are given, the following abbreviations are used: s, singlet; d, doublet; t, triplet; m, multiplet; b, broad. ^{13}C NMR spectra were proton decoupled and recorded on a 100 MHz Bruker spectrometer using the carbon signal of the deuterated solvent as the internal standard. UV-vis absorption spectra were recorded on a Cary 100 scan UV-vis spectrophotometer. Molecular weights of the polymers

were estimated by size exclusion chromatography on a single injection mode Polymer Laboratories PL-GPC 50 using THF as the mobile phase and toluene as the internal reference. The number-average molecular weights (M_n) were calibrated against PS standards, and the output was received and analyzed using an RI detector. Electrochemical measurements were performed on a BASi Epsilon potentiostat in anhydrous acetonitrile.

Mobility Measurements. Thin-film transistors were fabricated using heavily doped silicon substrates with 230 nm thermally grown SiO_2 (capacitance of 14.9 nF/cm^2). Gold electrodes were prepatterned onto the dioxide layer with channel lengths of 2.5, 5, 10, and $20 \mu\text{m}$. Prior to film deposition these substrates were cleaned with acetone and 2-propanol followed by oxygen plasma cleaning for 2 min. The cleaned substrates were then exposed to OTS vapors for at least 12 h at room temperature where the surface was modified by slow evaporation and condensation of the silane molecules. The substrates were then washed with anhydrous toluene and then heated at 80°C for 1 h to remove the unbound silanes. The substrates were then coated by spinning 10 mg/mL polymer solutions in anhydrous chlorobenzene (1500 rpm for 45 s) and annealed at 80°C for 1 h under a nitrogen atmosphere. The channel width was fixed at 10 mm for all devices. Field-effect mobility was estimated using a three-electrode Agilent 4156C precision semiconductor parameter analyzer.

Materials. All reagents were used as received without further purification, unless otherwise specified. All monomers and polymers were synthesized according to reported procedures with a few modifications wherever necessary. Air- and moisture-sensitive reactions were conducted in oven-dried glassware using a standard Schlenk line or drybox techniques under an inert atmosphere of dry nitrogen.

General Procedure for Polymerization via Sonogashira Polycondensation Reaction. A 5 mL pear-shaped Schlenk flask was charged with both monomers and a magnetic stirrer. The flask was then taken inside a glovebox maintained under an inert atmosphere of nitrogen. The catalyst $\text{Pd}(\text{PPh}_3)_4$ and cocatalyst (CuI) were added inside the glovebox. A 1:1 mixture of anhydrous diisopropylamine and anhydrous toluene was degassed using freeze-pump-thaw cycles. This degassed solvent mixture was then added to the monomers, and the reaction temperature was raised to 60°C . The polymerization was continued for 24 h. The polymers were then precipitated in excess methanol and isolated via gravity filtration. The crude polymers were then purified via continuous extraction using a Soxhlet apparatus. The monomers and the catalysts were removed by extraction with methanol. Acetone extraction removed the low molecular weight oligomers, and a

final chloroform extraction yielded the desired polymers. We found that in all polymerizations there remained a residue that was partly soluble in THF.

p(BODIPY). 2,6-DiiodoBODIPY (50 mg, 0.07 mmol) and 2,6-diethynylBODIPY (36 mg, 0.07 mmol) were added to a 5 mL Schlenk flask. Pd(PPh₃)₄ (6.0 mg, 5.2 μmol) and CuI (2.0 mg, 10.4 μmol) were added to the flask under nitrogen. A degassed mixture of anhydrous diisopropylamine (1.5 mL) and anhydrous toluene (1.5 mL) was added to the flask, and the polymerization was carried out according to the general procedure. The chloroform fraction was concentrated under reduced pressure to yield a deep violet colored polymer (48 mg). ¹H NMR (400 MHz, CDCl₃): δ 7.13 (br, 2H), 7.03 (br, 2H), 3.89 (br, 2H), 2.63 (s, 6H), 1.73 (br, 1H), 1.59 (s, 6H), 1.53–1.32 (br, 8H), 0.97 (br, 6H).

p(BODIPY-*alt*-Qx). Dibromoquinoxaline (23.0 mg, 0.08 mmol) and 2,6-diethynylBODIPY (40.0 mg, 0.08 mg) were added to a 5 mL Schlenk flask. Pd(PPh₃)₄ (6.0 mg, 5.2 μmol) and CuI (2.0 mg, 10.4 μmol) were added to the flask under nitrogen. A degassed mixture of anhydrous diisopropylamine (1.5 mL) and anhydrous toluene (1.5 mL) was added to the flask, and the polymerization was carried out according to the general procedure. The chloroform fraction was concentrated under reduced pressure and reprecipitated in methanol to yield a deep violet colored polymer (20 mg). ¹H NMR (400 MHz, CDCl₃): δ 8.98–8.91 (br, 2H), 8.09 (br, 2H), 7.05 (br, 4H), 3.91 (br, 2H), 2.66 (br, 6H), 1.55–1.10 (br, 23H), 0.89–0.83 (br, 6H).

p(BODIPY-*alt*-BzT). Dibromobenzothiadiazole (23.5 mg, 0.08 mmol) and 2,6-diethynylBODIPY (40.0 mg, 0.08 mg) were added to a 5 mL Schlenk flask. Pd(PPh₃)₄ (6.0 mg, 5.2 μmol) and CuI (2.0 mg, 10.4 μmol) were added to the flask under nitrogen. A degassed mixture of anhydrous diisopropylamine (1.5 mL) and anhydrous toluene (1.5 mL) was added to the flask, and the polymerization was carried out according to the general procedure. The chloroform fraction was concentrated under reduced pressure and reprecipitated in methanol to yield a deep violet colored polymer (40 mg). ¹H NMR (400 MHz, CDCl₃): δ 7.81 (br, 2H), 7.16 (br, 2H), 7.05 (br, 2H), 3.92 (br, 2H), 2.82–2.62 (br, 6H), 2.00 (br, 1H), 1.69 (br, 6H), 1.40–1.20 (m, 16H), 0.98–0.80 (br, 6H).

p(BODIPY-*alt*-NDI). 2,6-Dibromo-1,4,5,8-naphthalenetetracarboxylic-(2'-ethyl)hexyldiimide (52.0 mg, 0.08 mmol) and 2,6-diethynylBODIPY (40.0 mg, 0.08 mg) were added to a 5 mL Schlenk flask. Pd(PPh₃)₄ (6.0 mg, 5.2 μmol) and CuI (2.0 mg, 10.4 μmol) were added to the flask under nitrogen. A degassed mixture of anhydrous diisopropylamine (1.5 mL) and anhydrous toluene (1.5 mL) was added to the flask, and the polymerization was carried out according to the general procedure. The chloroform fraction was concentrated under reduced pressure and reprecipitated in methanol to yield a deep violet colored polymer (35 mg). ¹H NMR (400 MHz, CDCl₃): δ 8.77 (br, 2H), 7.09 (br, 4H), 4.12 (br, 4H), 3.94 (br, 2H), 2.65 (br, 6H), 1.77 (br, 3H), 1.55–1.25 (br, 24H), 0.95–0.85 (br, 18H).

p(BODIPY-*alt*-PDI). 1,7-Dibromo-3,4,9,10-perylenetetracarboxylic-(2'-ethyl)-hexyldiimide (62.0 mg, 0.08 mmol) and 2,6-diethynylBODIPY (40.0 mg, 0.08 mg) were added to a 5 mL Schlenk flask. Pd(PPh₃)₄ (6.0 mg, 5.2 μmol) and CuI (2.0 mg, 10.4 μmol) were added to the flask under nitrogen. A degassed mixture of anhydrous diisopropylamine (1.5 mL) and anhydrous toluene (1.5 mL) was added to the flask, and the polymerization was carried out according to the general procedure. The chloroform fraction was concentrated under reduced pressure and reprecipitated in methanol to yield a dark blue colored polymer (50 mg). ¹H NMR (400 MHz, CDCl₃): δ 9.63 (br, 2H), 8.42 (br, 6H), 7.09 (br, 4H), 4.15 (br, 6H), 2.79 (br, 6H), 1.34–1.23 (br, 30H), 0.93–0.91 (br, 18H).

■ ASSOCIATED CONTENT

● **Supporting Information.** Text giving detailed synthetic procedure, characterization, and figures showing NMR spectra

as well as output and transfer characteristic curves. This material is available free of charge via the Internet at <http://pubs.acs.org>.

■ AUTHOR INFORMATION

Corresponding Author

*E-mail: thai@chem.umass.edu.

■ ACKNOWLEDGMENT

We thank partial support from the U.S. Department of Energy through the EFRC at UMass Amherst (DE-SC0001087) and the U.S. Army Research Office (54635CH) through the Green Energy Center.

■ REFERENCES

- (1) Ulrich, G.; Ziessel, R.; Harriman, A. *Angew. Chem., Int. Ed.* **2008**, *47*, 1184–1201.
- (2) (a) Loudet, A.; Burgess, K. *Chem. Rev.* **2007**, *107*, 4891–4932. (b) Li, L.; Han, J.; Nguyen, B.; Burgess, K. *J. Org. Chem.* **2008**, *73*, 1963–1970.
- (3) Erten-Ela, S.; Yilmaz, M. D.; Icli, B.; Dede, Y.; Icli, S.; Akkaya, E. U. *Org. Lett.* **2008**, *10*, 3299–3302.
- (4) (a) Rousseau, T.; Cravino, A.; Bura, T.; Ulrich, G.; Ziessel, R.; Roncali, J. *Chem. Commun.* **2009**, 1673–1675. (b) Rousseau, T.; Cravino, A.; Bura, T.; Ulrich, G.; Ziessel, R.; Roncali, J. *J. Mater. Chem.* **2009**, *19*, 2298–2300. (c) Rousseau, T.; Cravino, A.; Ripaud, E.; Leriche, P.; Rihn, S.; De Nicola, A.; Ziessel, R.; Roncali, J. *Chem. Commun.* **2010**, 5082–5084.
- (5) Nagai, A.; Chujo, Y. *Macromolecules* **2010**, *43*, 193–200.
- (6) (a) Donuru, V. R.; Vegnesa, G. K.; Velayudham, S.; Green, S.; Liu, H. *Chem. Mater.* **2009**, *21*, 2130–2138. (b) Donuru, V. R.; Vegnesa, G. K.; Velayudham, S.; Meng, G.; Liu, H. *J. Polym. Sci., Part A: Polym. Chem.* **2009**, *47*, 5354–5366. (c) Donuru, V. R.; Zhu, S.; Green, S.; Liu, H. *Polymer* **2010**, *51*, 5359–5368. (d) Meng, G.; Velayudham, S.; Smith, A.; Luck, R.; Liu, H. *Macromolecules* **2009**, *42*, 1995–2001. (e) Zhu, M.; Jiang, L.; Yuan, M.; Liu, X.; Ouyang, C.; Zheng, H.; Yin, X.; Zuo, Z.; Liu, H.; Li, Y. *J. Polym. Sci., Part A: Polym. Chem.* **2008**, *46*, 7401–7410.
- (7) Kim, B.; Ma, B.; Donuru, V. R.; Liu, H.; Fréchet, J. M. J. *Chem. Commun.* **2010**, 4148–4150.
- (8) (a) Krumova, K.; Cosa, G. *J. Am. Chem. Soc.* **2010**, *132*, 17560–17569. (b) Collado, D.; Casado, J.; González, S. R.; Navarrete, J. T. L.; Suau, R.; Perez-Inestrosa, E.; Pappenfus, T. M.; Raposo, M. M. *Chem.—Eur. J.* **2011**, *17*, 498–507.
- (9) (a) Bundgaard, E.; Krebs, F. C. *Sol. Energy Mater. Sol. Cells* **2007**, *91*, 954–985. (b) Cheng, Y.-J.; Yang, S.-H.; Hsu, C.-S. *Chem. Rev.* **2009**, *109*, 5868–5923. (c) Chen, J.; Cao, Y. *Acc. Chem. Res.* **2009**, *42*, 1709–1718.
- (10) (a) Havinga, E. E.; ten Hoeve, W.; Wynberg, H. *Polym. Bull.* **1992**, *29*, 119–126. (b) Dhanabalan, A.; van Duren, J. K. J.; van Hal, P. A.; van Dongen; Janssen, R. A. J. *Adv. Funct. Mater.* **2001**, *11*, 255–262. (c) van Duren, J. K. J.; Dhanabalan, A.; van Hal, P. A.; Janssen, R. A. J. *Synth. Met.* **2001**, *121*, 1587–1588. (d) van Mullekom, H. A. M.; Vekemans, J. E. E.; Meijer, E. W. *Chem.—Eur. J.* **1998**, *4*, 1235–1243. (e) Ajayaghosh, A. *Chem. Soc. Rev.* **2003**, *32*, 181–191. (f) Zhang, F.; Mammo, W.; Andersson, L. M.; Adamassie, S.; Andersson, M. R.; Inganäs, O. *Adv. Mater.* **2006**, *18*, 2169–2173. (g) Zhu, Y.; Champion, R. D.; Jenekhe, S. A. *Macromolecules* **2006**, *39*, 8712–8719. (h) Li, Y.; Zou, Y. *Adv. Mater.* **2008**, *20*, 2952–2958. (i) Price, S. C.; Stuart, A. C.; You, W. *Macromolecules* **2010**, *43*, 4609–4612. (j) Zhang, X.; Steckler, T. T.; Dasari, R. R.; Ohira, S.; Potscavage, J. W. J.; Tiwari, S. P.; Coppée, S.; Ellinger, S.; Barlow, S.; Brédas, J.-L.; Kippelen, B.; Reynolds, J. R.; Marder, S. R. *J. Mater. Chem.* **2010**, *20*, 123–134. (k) Zhang, Y.; Hau, S. K.; Yip, H.-L.; Sun, Y.; Acton, O.; Jen, A. K.-Y. *Chem. Mater.* **2010**, *22*, 2696–2698.

- (11) (a) Kitamura, C.; Tanaka, S.; Yamashita, Y. *Chem. Mater.* **1996**, *8*, 570–578. (b) Perzon, E.; Wang, M.; Zhang, F.; Mammo, W.; Delgado, J. L.; de la Cruz, P.; Inganäs, O.; Langa, F.; Andersson, M. R. *Synth. Met.* **2005**, *154*, 53–56.
- (12) (a) Jayakannan, M.; van Hal, P. A.; Janssen, R. A. J. *J. Polym. Sci., Part A: Polym. Chem.* **2002**, *40*, 251–261. (b) Jayakannan, M.; van Hal, P. A.; Janssen, R. A. J. *J. Polym. Sci., Part A: Polym. Chem.* **2002**, *40*, 2360–2372. (c) Admassie, S.; Inganäs, O.; Mammo, W.; Perzon, E.; Andersson, M. R. *Synth. Met.* **2006**, *156*, 614–623. (d) Mühlbacher, D.; Scharber, M.; Morana, M.; Zhu, Z.; Waller, D.; Gaudiana, R.; Brabec, C. *Adv. Mater.* **2006**, *18*, 2884–2889. (e) Huo, L.; He, C.; Han, M.; Zhou, E.; Li, Y. *J. Polym. Sci., Part A: Polym. Chem.* **2007**, *45*, 3861–3871. (f) Peet, J.; Y., K. J.; Coates, N. E.; Ma, W. L.; Moses, D.; Heeger, A. J.; Bazan, G. C. *Nature Mater.* **2007**, *6*, 497–500. (g) Blouin, N.; Michaud, A.; Gendron, D.; Wakim, S.; Blair, E.; Neagu-Plesu, R.; Belletête, M.; Durocher, G.; Tao, Y.; Leclerc, M. *J. Am. Chem. Soc.* **2008**, *130*, 732–742. (h) Hou, J.; Chen, H.-Z.; Zhang, S.; Li, G.; Yang, Y. *J. Am. Chem. Soc.* **2008**, *130*, 16144–16145. (i) Lee, J. K.; Ma, W. L.; Brabec, C. J.; Yuen, J.; Moon, J. S.; Kim, J. Y.; Lee, K.; Bazan, G. C.; Heeger, A. J. *J. Am. Chem. Soc.* **2008**, *130*, 3619–3623. (j) Xiao, S.; Stuart, A. C.; Liu, S.; You, W. *ACS Appl. Mater. Interfaces* **2009**, *1*, 1613–1621.
- (13) (a) Wu, W.-C.; Liu, C.-L.; Chen, W.-C. *Polymer* **2006**, *47*, 527–538. (b) Gadisa, A.; Mammo, W.; Andersson, L. M.; Admassie, S.; Zhang, F.; Andersson, M. R.; Inganäs, O. *Adv. Funct. Mater.* **2007**, *17*, 3836–3842. (c) Lee, W.-Y.; Cheng, K.-F.; Wang, T.-F.; Chueh, C.-C.; Chen, W.-C.; Tuan, C.-S.; Lin, J.-L. *Macromol. Chem. Phys.* **2007**, *208*, 1919–1927. (d) Hou, J.; Park, M.-H.; Zhang, S.; Yao, Y.; Chen, L.-M.; Li, J.-H.; Yang, Y. *Macromolecules* **2008**, *41*, 6012–6018. (e) Liu, C.-L.; Tsai, J.-H.; Lee, W.-Y.; Chen, W.-C.; Jenekhe, S. A. *Macromolecules* **2008**, *41*, 6952–6959. (f) Karsten, B. P.; Bijleveld, J. C.; Viani, L.; Cornil, J.; Gierschner, J.; Janssen, R. A. J. *J. Mater. Chem.* **2009**, *19*, 5343–5350. (g) Lai, M.-H.; Chueh, C.-C.; Chen, W.-C.; Wu, J.-L.; Chen, F.-C. *J. Polym. Sci., Part A: Polym. Chem.* **2009**, *47*, 973–985. (h) Chen, C.-H.; Hsieh, C.-H.; Dubosc, M.; Cheng, Y.-J.; Hsu, C.-S. *Macromolecules* **2010**, *43*, 697–708. (i) Tsai, J.-H.; Lee, W.-Y.; Chen, W.-C.; Yu, C.-Y.; Hwang, G.-W.; Ting, C. *Chem. Mater.* **2010**, *22*, 3290–3299. (j) Wang, E.; Hou, L.; Wang, Z.; Hellström, S.; Zhang, F.; Inganäs, O.; Andersson, M. R. *Adv. Mater.* **2010**, *22*, 5240–5244. (k) Zheng, Q.; Jung, B. J.; Sun, J.; Katz, H. E. *J. Am. Chem. Soc.* **2010**, *132*, 5394–5404. (l) Zhou, E.; Cong, J.; Yamakawa, S.; Wei, Q.; Nakamura, M.; Tajima, K.; Yang, C.; Hashimoto, K. *Macromolecules* **2010**, *43*, 2873–2879.
- (14) (a) Campos, L. M.; Tontcheva, A.; Günes, S.; Sonmez, G.; Neugebauer, H.; Sariciftci, N. S.; Wudl, F. *Chem. Mater.* **2005**, *17*, 4031–4033. (b) Zhu, Y.; Champion, R. D.; Jenekhe, S. A. *Macromolecules* **2006**, *39*, 8712–8719. (c) Zoombelt, A. J.; Gilot, J.; Wienk, M. M.; Janssen, R. A. J. *Chem. Mater.* **2009**, *21*, 1663–1669. (d) Ashraf, R. S.; Gilot, J.; Janssen, R. A. J. *Sol. Energy Mater. Sol. Cells* **2010**, *94*, 1759–1766.
- (15) (a) Karikomi, M.; Kitamura, C.; Tanaka, S.; Yamashita, Y. *J. Am. Chem. Soc.* **1995**, *117*, 6791–6792. (b) Steckler, T. T.; Abboud, K. A.; Craps, M.; Rinzler, A. G.; Reynolds, J. R. *Chem. Commun.* **2007**, 4904–4906. (c) Qian, G.; Dai, B.; Luo, M.; Yu, D.; Zhan, J.; Zhang, Z.; Ma, D.; Wang, Z. Y. *Chem. Mater.* **2008**, *20*, 6208–6216.
- (16) (a) Cai, T.; Zhou, Y.; Wang, E.; Hallström, S.; Zhang, F.; Xu, S.; Inganäs, O.; Andersson, M. R. *Sol. Energy Mater. Sol. Cells* **2010**, *94*, 1275–1281. (b) Dallos, T.; Hamburger, M.; Baumgarten, M. *Org. Lett.* **2011**, *13*, 1936–1939.
- (17) (a) Jung, B. J.; Sun, J.; Lee, T.; Sarjeant, A.; Katz, H. E. *Chem. Mater.* **2009**, *21*, 94–101. (b) Katz, H. E.; Lovinger, A. J.; Johnson, J.; Kloc, C.; Siegrist, T.; Li, W.; Lin, Y.-Y.; Dodabalapur, A. *Nature* **2000**, *404*, 478–481. (c) Guo, X.; Watson, M. D. *Org. Lett.* **2008**, *10*, 5333–5336.
- (18) (a) Kolhe, N. B.; Asha, S. K.; Senanayak, S. P.; Narayan, K. S. *J. Phys. Chem. B* **2010**, *114*, 16694–16704. (b) Schmidt, R.; Oh, J. H.; Sun, Y.-S.; Deppisch, M.; Krause, A.-M.; Radacki, K.; Braunschweig, H.; Könemann, M.; Erk, P.; Bao, Z.; Würthner, F. *J. Am. Chem. Soc.* **2009**, *131*, 6215–6228.
- (19) Gawrys, P.; Boudinet, D.; Zagorska, M.; Djurado, D.; Verilhac, J.-M.; Horowitz, G.; Pécaud, J.; Pouget, S.; Pron, A. *Synth. Met.* **2009**, *159*, 1478–1485.
- (20) (a) Yan, H.; Chen, Z.; Zheng, Y.; Newman, C.; Quinn, J. R.; Dötz, F.; Kastler, M.; Facchetti, A. *Nature* **2009**, *457*, 679–687. (b) Kim, F. S.; Guo, X.; Watson, M. D.; Jenekhe, S. A. *Adv. Mater.* **2010**, *22*, 478–482. (c) Chen, Z.; Zheng, Y.; Yan, H.; Facchetti, A. *J. Am. Chem. Soc.* **2009**, *131*, 8–9. (d) Durban, M. M.; Kazarinoff, P. D.; Luscombe, C. K. *Macromolecules* **2010**, *43*, 6348–6352.
- (21) (a) Zhan, X.; Tan, Z.; Zhou, E.; Li, Y.; Misra, R.; Grant, A.; Domercq, B.; Zhang, X.-H.; An, Z.; Zhang, X.; Barlow, S.; Kippelen, B.; Marder, S. R. *J. Mater. Chem.* **2009**, *19*, 5794–5803. (b) Zhan, X.; Tan, Z.; Domercq, B.; An, Z.; Zhang, X.; Barlow, S.; Li, Y.; Zhu, D.; Kippelen, B.; Marder, S. R. *J. Am. Chem. Soc.* **2007**, *129*, 7246–7247.
- (22) Goze, C.; Ulrich, G.; Ziesel, R. *Org. Lett.* **2006**, *8*, 4445–4448.
- (23) Mancilha, F. S.; DaSilveira Neto, B. A.; Lopes, A. S.; Moreira, P. F., Jr.; Quina, F. H.; Gonçalves, R. S.; Dupont, J. *Eur. J. Org. Chem.* **2006**, *2006*, 4924–4933.
- (24) (a) Piyakulawatt, P.; Keawprajak, A.; Chindaduang, A.; Hanusch, M.; Asawapirom, U. *Synth. Met.* **2009**, *159*, 467–472. (b) Yue, W.; Zhen, Y.; Li, Y.; Jiang, W.; Lv, A.; Wang, Z. *Org. Lett.* **2010**, *12*, 3460–3463.
- (25) (a) Vajiravelu, S.; Ramunas, L.; Vidas, G. J.; Valentas, G.; Vyginta, J.; Valiyaveetil, S. J. *Mater. Chem.* **2009**, *19*, 4268–4275. (b) Würthner, F.; Stepanenko, V.; Chen, Z.; Saha-Möllner, C. R.; Kocher, N.; Stalke, D. *J. Org. Chem.* **2004**, *69*, 7933–7939.
- (26) Huo, L.; Zhou, Y.; Li, Y. *Macromol. Rapid Commun.* **2008**, *29*, 1444–1448.
- (27) Pommerehne, J.; Vestweber, H.; Guss, W.; Mahrt, R. F.; Bäessler, H.; Porsch, M.; Daub, J. *Adv. Mater.* **1995**, *7*, 551–554.
- (28) Kondratenko, M.; Moiseev, A. G.; Perepichka, D. F. *J. Mater. Chem.* **2011**, *21*, 1470–1478.
- (29) Lee, S. K.; Zu, Y.; Herrmann, A.; Geerts, Y.; Müllen, K.; Bard, A. J. *J. Am. Chem. Soc.* **1999**, *121*, 3513–3520.
- (30) (a) Huang, J.; Wu, Y.; Fu, H.; Zhan, X.; Yao, J.; Barlow, S.; Marder, S. R. *J. Phys. Chem. A* **2009**, *113*, 5039–5046. (b) Hung, Y.-C.; Jiang, J.-C.; Chao, C.-Y.; Su, W.-F.; Lin, S.-T. *J. Phys. Chem. B* **2009**, *113*, 8268–8277. (c) Zhang, X.; Steckler, T. T.; Dasari, R. R.; Ohira, S.; Potscavage, J. W. J.; Tiwari, S. P.; Coppée, S.; Ellinger, S.; Barlow, S.; Brédas, J.-L.; Kippelen, B.; Reynolds, J. R.; Marder, S. R. *J. Mater. Chem.* **2010**, *20*, 123–134. (d) Steckler, T. T.; Zhang, X.; J., H.; Honeyager, R.; Ohira, S.; Zhang, X.-H.; Grant, A.; Ellinger, S.; Odom, S. A.; Sweat, D.; Tanner, D. B.; Rinzler, A. G.; Barlow, S.; Brédas, J.-L.; Kippelen, B.; Marder, S. R.; Reynolds, J. R. *J. Am. Chem. Soc.* **2009**, *131*, 2824–2826.